Investigating Nonlinear Viscoelastic Properties of Molten Carbon Black/Poly(ethylene-*co*-butyl acrylate) Composites, Using Fourier Transform Rheometry and Other Test Techniques

Jean L. Leblanc,[1] Karl-Michel Jäger[2]

[1]*Polymer Rheology and Processing, Universite Pierre & Marie Curie (Paris 6), 60, rue Auber-F-94408 Vitry-sur-Seine, France*
[2]*Marketing and Development Centre Wire and Cable, Borealis AB, 444 86 Stenungsund, Sweden*

Received 26 November 2005; accepted 29 July 2005
DOI 10.1002/app.23274
Published online in Wiley InterScience (www.interscience.wiley.com).

ABSTRACT: A series of molten carbon black (CB)/poly(ethylene-*co*-butyl acrylate) (EBA) composites were investigated through Fourier transform (FT) rheometry and other techniques. Filler loadings were above the critical percolation value, and consequently, strongly nonlinear viscoelastic properties were observed, with, in addition, an unusual complexity of carbon black effects when compared with other systems, for instance filled elastomers. FT rheometry appears particularly sensitive to such a complexity with typical variations of torque harmonics, as dynamic torsional strain is increased at constant frequency and temperature. How CB particles are distributed in the material appears as the key to understand experimental results. Indeed, in CB–EBA composites, filler particles concentrate in amorphous regions of the polymer, which are also butyl acrylate (BA)-rich regions. At room temperature, such composites are basically dual-phase systems: ethylene segments (PE)-rich crystallites and CB-rich amorphous BA regions. Solid-state mechanical properties reflect this morphology. As temperature increases, crystallites melt down allowing a pseudofluid state to be eventually reached but the dual-phase morphology is essentially kept. It follows that, under increasing (dynamic) strain, such complex dual-phase molten systems exhibit a response that initially reflects a contribution from PE-rich regions, easier to deform than CB-rich amorphous BA regions, before the expected response of the filled BA phase is observed. J Appl Polym Sci 101: 4071–4082, 2006

Key words: carbon black; poly(ethylene-*co*-butyl acrylate); composites; Fourier transform rheometry; morphology

INTRODUCTION

Semiconducting power cable shielding is an application for complex polymer systems that requires highly loaded carbon black (CB) composites. For such applications, loadings up to 40 wt % are quite common in thermoplastic polymers but an excellent dispersion of the filler is required to achieve an optimal microstructure and hence a smooth extruded surface as well as adequate conductive properties. In term of filler volume fraction, such loadings are above the critical value of percolation theory, i.e., $\Phi_c \approx 0.14-0.17$. Consequently such filled composites are expected to exhibit a set of interesting nonlinear viscoelastic properties, not only in the solid (i.e., at room temperature), but also in the molten state.

In composites made by mixing CB particles with poly(ethylene-*co*-butyl acrylate) (EBA), semiconducting properties depend on a CB network microstructure or, in other words, on filler–filler interactions. CB microstructure in EBA composites can be improved evolve when materials are held above their melting temperature, but with modified electrical properties after cooling.[1] But polymer–filler interactions might also be suspected, which would help to stabilize the morphology of the material during processing operations. Jäger and Eggen[2] have recently reported melt rheology data obtained with a Rheometrics dynamic analyzer (RDA), at constant strain (5%) and temperature (190°C), on a series of composites with various types of CB in the loading range 25–40 wt %. They clearly detected nonlinear effects, such as the disappearance of the so-called Newtonian plateau on the (dynamic) viscosity function, in sharp contrast with the pure, unfilled polymer. They treated their data to extract yield stress values, which they used as an indication of CB network structure and strength. As they commented, however, dynamic testing with instrument like the RDA is however strictly valid, providing linear viscoelastic behavior is observed, which is practically never the case with filled materials as outlined elsewhere.[3,4]

Correspondence to: J. L. Leblanc (jean.leblanc@ccr.jussieu.fr).

TABLE I
Test Composites

Sample coding	EBA00	EBA13	EBA14	EBA15	EBA16	EBA19	EBA28
Poly(ethylene-*co*-butyl acrylate)[a]	100	66.8	63.7	60.9	57.5	60.7	61.0
Furnace CB 1[b]	–	33.2	36.3	39.1	42.5	–	–
Furnace CB 2[c]	–	–	–	–	–	39.3	–
Acetylene black[d]	–	–	–	–	–	–	39.0
Φ^{e}_{black}	0	0.203	0.226	0.248	0.275	0.249	0.247
Measured ρ (g/cm^3)	0.924	1.082	1.112	1.139	1.152	1.134	1.138

[a] 4 mol % butyl acrylate; high pressure process as for LDPE; MFI 18 (190°C; 2.16 kg).
[b] DBPA: 100–120 mL/100 g; iodine number: 150–170 mg/g.
[c] DBPA: 110–130 mL/100 g; iodine number: 70–90 mg/g.
[d] DBPA: 200–220 mL/100 g, iodine number: 80–100 mg/g.
[e] Specific gravity data used in calculation (g/cm^3): EBA 0.923; N330 1.80.

Fourier transform (FT) rheometry is a development of so-called dynamic (or harmonic) testing that allows to accurately investigate both the linear and the nonlinear viscoelastic domains of polymer materials. Contrary to standard dynamic testing, for which strict proportionality between stress and strain is required for valid resolution of the (measured) complex modulus into its elastic and viscous components, FT rheometry is not restricted to the linear domain. Therefore, this new technique suits particularly well for complex polymer systems whose main characteristic is generally a strong nonlinear viscoelastic behavior. The objectives of the cooperative work reported here were to investigate the rheological properties of a series of CB/EBA composites, through FT rheometry and other techniques.

EXPERIMENTAL

Test materials

A series of filled composites, as described in Table I, were prepared in a pilot scale Buss extruder with a small amount of antioxidant. Pellets were then compression molded to 1.5-mm thick plates, out of which samples were die-cut.

Test methods

Dynamic mechanical testing (in solid state)

A dynamic mechanical analyser (Rheometrics, ARES) was used to perform strain sweep experiments at 23°C and constant frequency (1 Hz; 6.28 rad/s), in rectangular torsion mode. The samples were about 23-mm long, 9.9-mm wide, and 1.1–1.5-mm thick.

Standard dynamic testing (in molten state)

The experiments were carried out in a RDA II in plate–plate configuration at 190°C applying a frequency sweep with a strain of 5%. This strain amplitude has been chosen since it appeared to be the smallest amplitude that resulted in reasonable measurement accuracy.

Ft rheometry (molten state)

Rpa-ft and sample loading

A purposely modified Rubber Process Analyzer RPA® (Alpha Technologies) was used to perform FT rheometry experiments. As described elsewhere, strain and torque signals are captured using an appropriate software developed in LabView®, then FT calculation techniques are applied to the captured signals to resolve them in their main component and other harmonics, if any.[5,6] Any dynamic rheometer can conveniently be modified for FT testing but, owing to its closed cavity, the RPA allows quite large strain amplitude to be applied.

With respect to its measuring principle, the RPA cavity must be loaded with a slight volume excess of test material. The theoretical cavity volume is 3280 mm^3 and, by considering a volume excess of 5%, optimized sample loadings were calculated with respect to the measured specific gravities of the composites, i.e., from 3.18 g for EBA00 up to 3.97 g for EBA16. Samples for RPA testing were prepared by die cutting 46-mm diameter disks out of molded plates. Each sample was weighed and, if necessary, adjusted to maintain its weight within the optimized loading $\pm$0.2 g.

Protocols for strain sweep experiments

Strain sweep tests were performed with the RPA, according to protocols given in Table II. Each protocol describes strain sweep experiments through two subsequent runs separated by a resting period of 2 min. At least two samples of the same material were tested, using protocols named "Ssweep 1Hz A" and "Ssweep 1Hz B" such that, through inversion of the strain sequences (i.e., run 1 and run 2), sample fatigue effects would be detected, if any. At each strain sweep step, data acquisition was made recording

TABLE II
RPA Strain Sweep Test Protocols

Test protocol	Strain (deg) Run 1	Run 2
Ssweep_1Hz_A	0.5	0.6
	1	1.5
	2.5	3.5
	5	6.7
	8.5	10
	12	14.5
	17	20
	22.5	25
	27.5	30
	31.5	33
Ssweep_1Hz_B	0.6	0.5
	1.5	1
	3.5	2.5
	6.7	5
	10	8.5
	14.5	12
	20	17
	25	22.5
	30	27.5
	33	31.5

RPA test conditions – temperature, 200°C; frequency, 1 Hz. Sample conditioning – preheating, 3 min, at rest; fixing: 30 s, 1 Hz, 0.20°; preheating: 2 min, at rest. Resting period between runs, 2 min.

10,240 points at the rate of 512 point/s. Twenty cycles were consequently recorded at each strain step with the RPA set to apply a sufficient number of cycles (i.e., 40) for the steady harmonic regime to be reached.

With the protocols described in Table II, two subsequent strain sweep tests are performed within the limits of the instrument, at the frequency considered, to capture signals up to the far nonlinear region, with evidence for strain sensitivity of the material, if any. An experiment lasts for about 23 min and two samples are tested using the two protocols in such a manner that the strain sequences of the successive runs are inverted. If the tested material is sensitive to strain amplitude, differences are seen between runs 1 and 2, with the strain range documented by 20 data points. Such an experimental approach was designed to obtain the maximum number of data in the shortest test time (1 h), while documenting in the meantime the test repeatability and the material homogeneity.

Fourier transform analysis

The modified RPA yields both strain and torque signals as recorded data files of actual harmonic strain and stress readings versus time. A specific calculation program, written using the FT algorithm available in MathCad 8.0® (MathSoft Inc.), is used to obtain the amplitude of the main stress and strain components (corresponding the test frequency) and the relative magnitudes (in %) of the odd-harmonic components, i.e., $I(n\times\ \omega_1)/I(\omega_1)$.* The number of data points used, the frequency resolution (Hz), the acquisition time (s), and the sampling rate (point/s) are also provided. Figure 1 shows the averaged torque signal recorded when submitting an EBA/CB composite (i.e., sample EBA016) to 31.5° strain, at 1 Hz. As can be seen, the signal is harmonic but clearly distorted in comparison with a sinusoid of same amplitude. The displayed torque signal was averaged out of 20 recorded cycles (i.e., 10,240 data points) and the standard deviation drawn as a shaded area is barely visible, which demonstrates the excellent stability of the torque response. The single FT spectrum, obtained through calculation on the last 8192 points of the recorded torque (upper left in the figure), exhibits significant odd harmonics. The inserted table gives the results of the odd harmonic components analysis on both the torque and strain signals. The very low strain harmonic peaks (<0.13%) indicate the excellent quality of the applied signal at this strain angle.

Standard capillary rheometry

Capillary rheometry was performed at 190°C, using a Rosand Capillary Rheometer with a die having a length of 20 mm and a diameter of 1 mm. The melt was preheated for 10 min. The uncorrected shear rate was varied between 20 and 800 s^{-1}. The so-called Rabinowitsch correction for non-Newtonian character was applied to yield true shear rate data.

RESULTS

Complex modulus at room temperature

Figure 2 shows the effect of strain amplitude on the complex modulus measured at room temperature. Strain sweep allows to clearly detect a linear viscoelastic region, whose extent depends on filler loading, as expected. Both the effect of CB loading (left graph) and structure (right graph) are well seen, and, by drawing horizontal lines through the flat region of the curves, complex modulus data at zero strain are easily determined. As expected, the higher the filler loading, the higher the zero strain modulus, and as shown in the middle insert the volume fraction effect would correspond to a Guth, Gold, and Simha model,[7,8] slightly modified with a factor f to account for an effective volume concept taking qualitatively the complex filler geometry into account, as reviewed by

*Note that in this paper, $I(n\omega_1)/I(\omega_1)$ or the abridged form $I(n/1)$, is used to describe the nth relative harmonic component of any harmonic signal; $S(n\omega_1)/S(\omega_1)$ or $S(n/1)$ specifically means that a strain signal is considered; $T(n\omega_1)/T(\omega_1)$ or $T(n/1)$ is used for the torque signal.

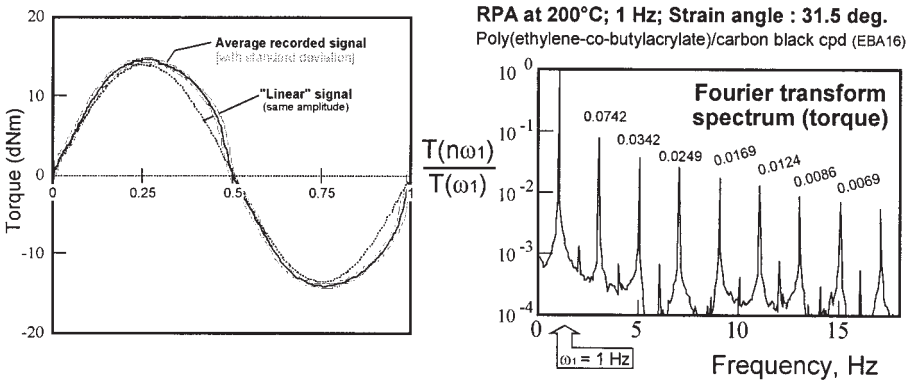

Fourier transform spectrum; odd harmonic components analysis

Nr pts	Freq.resol	Main freq.	3rd harm.	5th harm.	7th harm.	9th harm.	11th harm.	13th harm.	15th harm.
t_{aq}	Sampling pt/s	Main Torque a.u.	T(3/1), %	T(5/1), %	T(7/1), %	T(9/1), %	T(11/1), %	T(13/1), %	T(15/1), %
		Main Strain a.u.	S(3/1), %	S(5/1), %	S(7/1), %	S(9/1), %	S(11/1), %	S(13/1), %	S(15/1), %
8.192	0.063	**1**	3	5	7	9	11	13	15
7.998	512	**693**	7.42	3.42	2.49	1.69	1.24	0.86	0.69
		1435	0.13	007	0.05	0.05	0.02	0.02	0.01

Figure 1 Typical results from FT rheometry.

Wolff and Wang.[9] The dash curve in the middle insert was drawn using the following equation:

$$G^*_{cpd} = G^*_{matrix}(1 + 2.5 \times f \times \Phi_{filler} + 14.1 \times f^2 \times \Phi^2_{filler}) \quad (1)$$

with G_{matrix}^* = 40 MPa and f = 1.74. Despite the limited volume fraction range, the excellent application of eq. (1) to experimental data would suggest that, at least for the CB considered, the reinforcing effect in the solid state is essentially hydrodynamic. The applicability of this equation has been reported earlier in similar systems.[1]

The right-side graph in Figure 2 displays the effect of CB type at same loading. Interestingly, it appears that the reinforcing effect of the CB is determined by the CB surface area rather than by the complexity of the aggregate structure. This is somewhat surprising, since it is commonly considered that the factor f increases with the DBPA number,[9] which in the case of filled rubber compounds has been interpreted as being due to an effective filler volume due to some polymer being trapped between the branches of CB aggregates. The contrary is observed in the systems studied here. Rather than the specific surface area (i.e., comparing

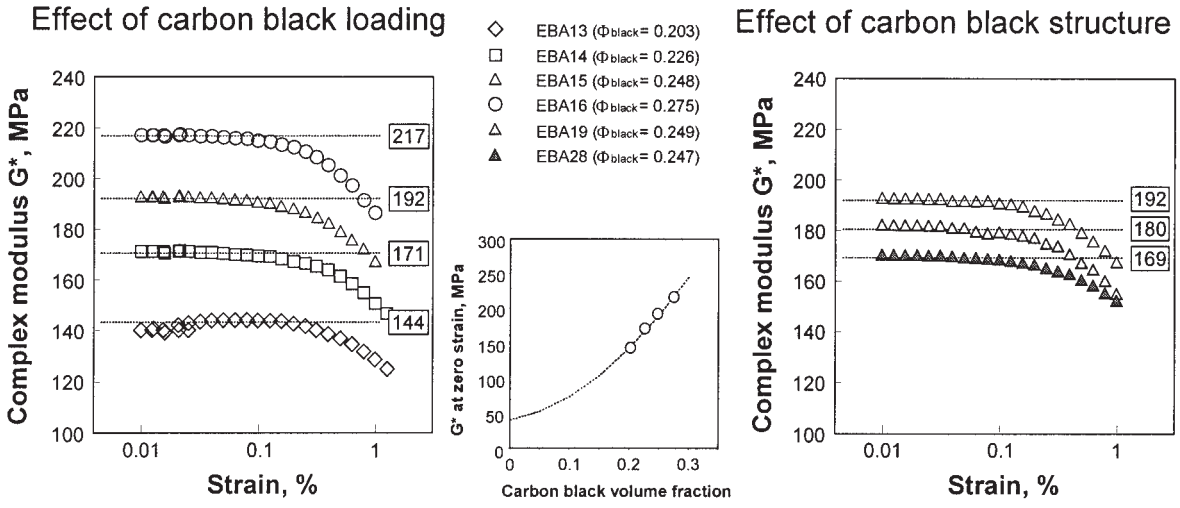

Figure 2 Complex modulus versus strain at room temperature of EBA/CB composites.

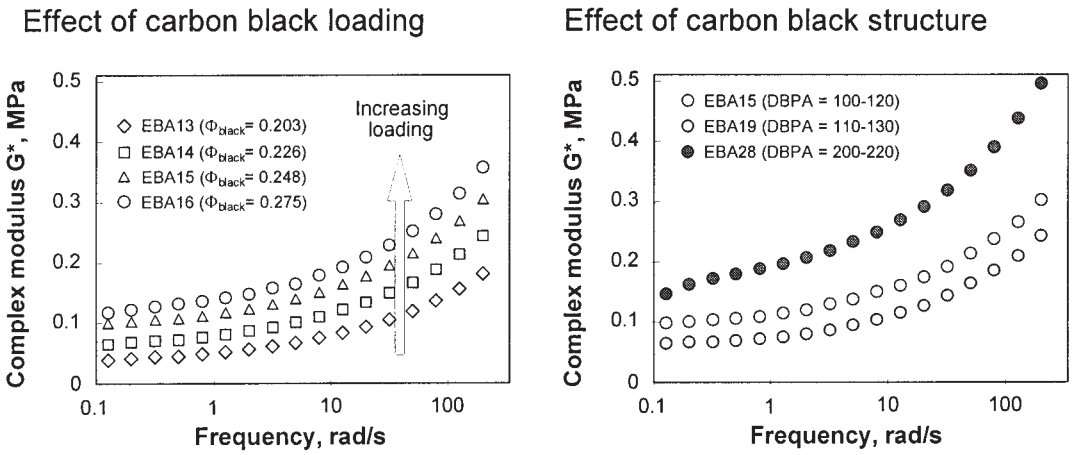

Figure 3 Complex modulus versus strain at 190°C of EBA/CB composites, using standard dynamic testing (RDA II).

furnace black 1 compound, EBA15, with furnace black 2 compound, EBA19) and/or the surface activity (comparing furnace black with acetylene black) it seems that filler–polymer interfacial effects have the most significant contribution. Such results should therefore be considered in terms of effective filler fraction (i.e., carbon particle + immobilized polymer) rather than with respect to particle anisometry effects because a significant part of the polymer is probably either entrapped within or at least strongly interacting with carbon black aggregates.

Dynamic mechanical testing and capillary rheometry at 190°C

Dynamic behavior as assessed in the molten state with a standard rheometer is shown in Figure 3. The effect of CB loading is clearly seen with the furnace black 1 series (samples EBA13–EBA16). However, the reinforcing character of the different CB types (right graph) is different compared with the observation in the solid state (Fig. 2). In contrast, the high structure acetylene black (EBA28) imparts now the higher modulus to the composite in molten state. However, the low structure/high surface furnace black 1 reinforces stronger than the furnace black 2 having a higher structure and a smaller surface area. Interestingly, this picture becomes completely reversed in capillary rheometry measurements that shows a clear ranking according to the DBPA number, as illustrated in the right part of Figure 4. Altogether, this suggests that the reinforcing mechanism of CB in our systems is largely affected not only by the temperature but also by the flow conditions.

FT rheometry results

Harmonic strain signal quality

Ideal dynamic testing requires that a perfect sinusoidal deformation at controlled frequency and strain can be applied on the test material. In the RPA, the (har-

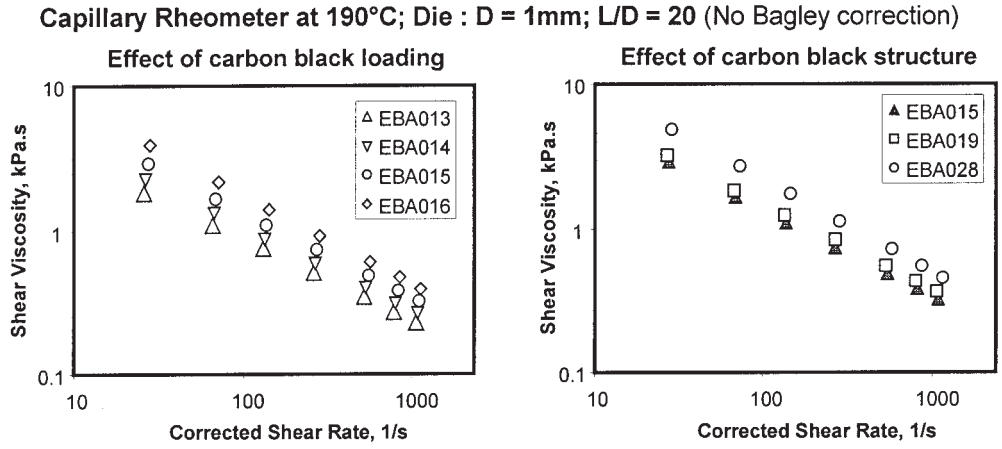

Figure 4 Capillary rheometer results at 190°C of EBA/CB composites.

monic) strain of the material occurs by means of an oscillating wall, i.e., the lower die, through the monitored operation of a high precision motor with a complex electronics. Whatever be the quality of design and manufacturing of a dynamic rheometer, there are always technical limits in accurately producing the harmonic mechanical motion. Fast FT of the strain (i.e., applied) signal allows this aspect to be documented, since no (significant) harmonics would be found if the strain signal were perfect.

RPA strain signal quality was previously documented in detail, by capturing signals in various conditions, first when the cavity is empty and second when it is loaded with materials of increasing stiffness (in fact a series of carbon black filled polybutadiene compounds). As expected a linear relationship was observed between the set strain angle and the main strain component (in arbitrary units) revealed by FT analysis, whatever the test conditions were, thus demonstrating that, in terms of strain crest signal, the maximum oscillation angle of the lower die can be considered as nearly perfect. The same conclusion is drawn from the data obtained in the present study.

Depending on the set strain amplitude, FT analysis however reveals significant (i.e., larger than noise) odd harmonics components, with obviously the third harmonic the larger one. When the cavity is empty, it was previously observed that the third relative harmonic strain component, i.e., $S(3/1)$, decreases with the strain angle and pass below 1% of the main component when it is higher than 1.3–1.5°. Data obtained in various conditions allowed to show that a simple three-parameters hyperbolic decay equation, i.e., $S(3/1) = \mathrm{S}(3/1)=a + \frac{bc}{c+\gamma}$, with $a = 0.086$, $b = 4.31$, and $c = 0.408$, was expressing well the strain signal quality dependence on set strain angle. With very stiff materials, loading the cavity was found to significantly affect the strain signal quality, as reflected by the relative third harmonic strain component. As shown in Figure 5, no such effect is seen with EBA composites with increasing filler loading, likely due to the low stiffness of such materials at the test temperature. When the strain angle is higher than 1.5–1.6° (around 25% deformation), $S(3/1)$ is below 1%, and moreover, the strain signal quality improves as the applied deformation increases.

Main torque component

Results obtained on two samples of the same test material superimpose well, which demonstrates their excellent homogeneity. Some difficulties were met with the unfilled material (EBA00) owing to its very low stiffness; at very low strain angle, no significant torque signal was obtained and data were discarded. Figure 6 shows how main torque components $T(\omega_1)$ varies with the set strain γ for composites with increasing level of furnace CB. Strong nonlinearity is observed and, in the low strain region, the curves for filled EBA samples do not converge to zero. The unfilled material (EBA00) exhibits a significantly different behavior that needs magnification to be clearly seen (Fig. 7).

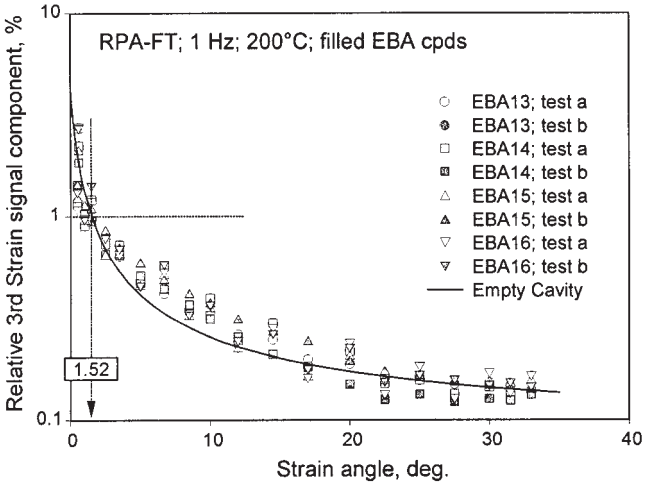

Figure 5 Applied strain signal quality through third harmonic signal component.

Figure 7 clearly shows that, in the low strain region, the $T(\omega_1)$ versus γ curve of the pure EBA reduces to a straight line that can be extrapolated to zero; in other terms, this material clearly exhibit a linear behavior. The filled composite is notably different. First, the material is (slightly) shear sensitive, as demonstrated by the nonsuperposition of data from runs 1 and 2. Second, no extrapolation toward zero is possible.

The ratio $T(\omega_1)/\gamma$ has obviously the meaning of a modulus and, for materials that have a linear viscoelastic region, plotting this quantity versus strain would yield the most familiar picture of a plateau region at low strain, then typical strain dependence. Figure 8 shows that it is indeed the case for the pure EBA sample, but that the filled EBA has no linear viscoelastic region with the low strain modulus tending to increase to very large values as strain amplitude decrease. Note that with respect to the data acquisition conditions used for FT calculation, the following equality holds: G^* (kPa) = 12.335 × $T(\omega_1)/\gamma$ (with $T(\omega_1)$ in arbitrary unit and γ in %).

As with other unfilled polymers, the classical curve obtained with the pure EBA (see the lower left insert in Fig. 8 for a magnification) can adequately be modeled with the following simple equation:

$$\frac{T(\omega_1)}{\gamma} = \left[\frac{T(\omega_1)}{\gamma}\right]_0 \times \left[\frac{1}{1+(A\gamma)^B}\right] \qquad (2)$$

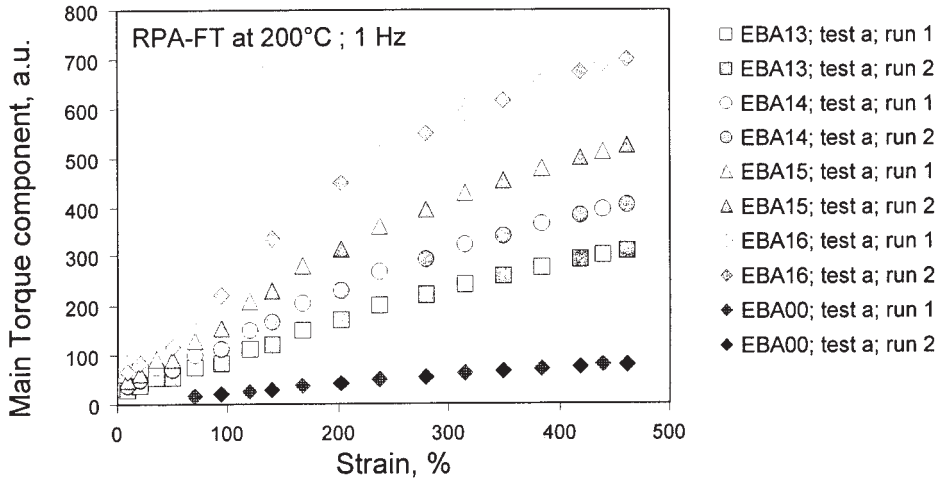

Figure 6 Main torque component $T(\omega_1)$ versus strain for EBA composites with increasing levels of furnace carbon black; data on pure EBA is shown for comparison.

where $\left[\frac{T(\omega_1)}{\gamma}\right]_0$ is the modulus in the linear region, A the reverse of a critical strain marking the limit between the linear and nonlinear regions, and B a parameter describing the strain sensitivity of the material (see Table III). The so-derived linear modulus is obviously the initial slope of the $T(\omega_1)$ versus γ, and strictly corresponds to the linear viscoelastic behavior of the material. With respect to the scale used in the insert, no difference is seen between data gathered through runs 1 and 2, thus demonstrating that the unfilled EBA is not sensitive to strain history or that any memory effect is conveniently damped down during the resting period (2 min) between the two runs.

Figure 9 shows that this model does not meet the data obtained with the EBA composites, which moreover exhibit a pretty unusual behavior, in full contrast with the experience gained so far with filled rubber compounds and FT rheometry.[10] As reported by various authors, CB- and silica-filled rubber compounds exhibit reduced linear viscoelastic regions with increasing filler loading, until simple proportionality between stress and strain ceases to be observed within the available strain window.[3,6] EBA/CB composites exhibit no linear region at vanishing strain, and furthermore, nonlinearity increases as strain amplitude decreases. In addition, the higher the filler content, the larger the strain history effect, as reflected by the difference between runs 1 and 2.

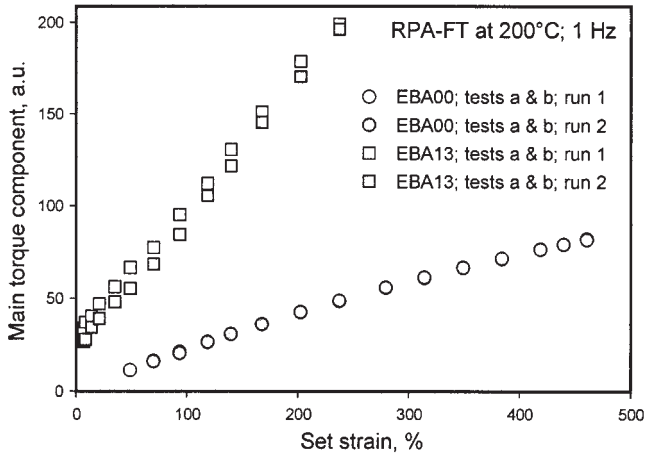

Figure 7 Comparing the main torque component versus strain for pure and filled EBA.

Redrawing Figure 9 with log–log scales allows an interesting observation to be made (note that only run 1 results were used for clarity). As shown in Figure 10, beyond a strain of ~120%, the $T(\omega_1)/\gamma$ ratio decrease of filled EBA composites is qualitatively similar to the curve for the pure EBA, except a vertical shift that depends on the carbon black loading. The high strain nonlinearity of filled EBA can consequently be modeled using eq. (2) (see results in Table IV and the corresponding traces in Fig. 10; note that only data gathered with strain higher than 90% were used in fitting eq. (2)). The nonlinearity in the low strain region (i.e., below 100%) of filled EBA composites seems to correspond to a mere power law decrease, and a vertical shift due to CB loading.

Data in Table IV show that the (extrapolated) modulus $\left[\frac{T(\omega_1)}{\gamma}\right]_0$ increases with carbon black content, roughly in an exponential manner, markedly different from the Guth, Gold, and Simha model previously mentioned, which considers essentially mere hydrodynamic interactions between the matrix and the dispersed particles. The parameter B, which expresses the (high) strain sensitivity, tends to marginally increases with filler loading, and the reverse of A shows that the higher the CB level the lower the strain at which high

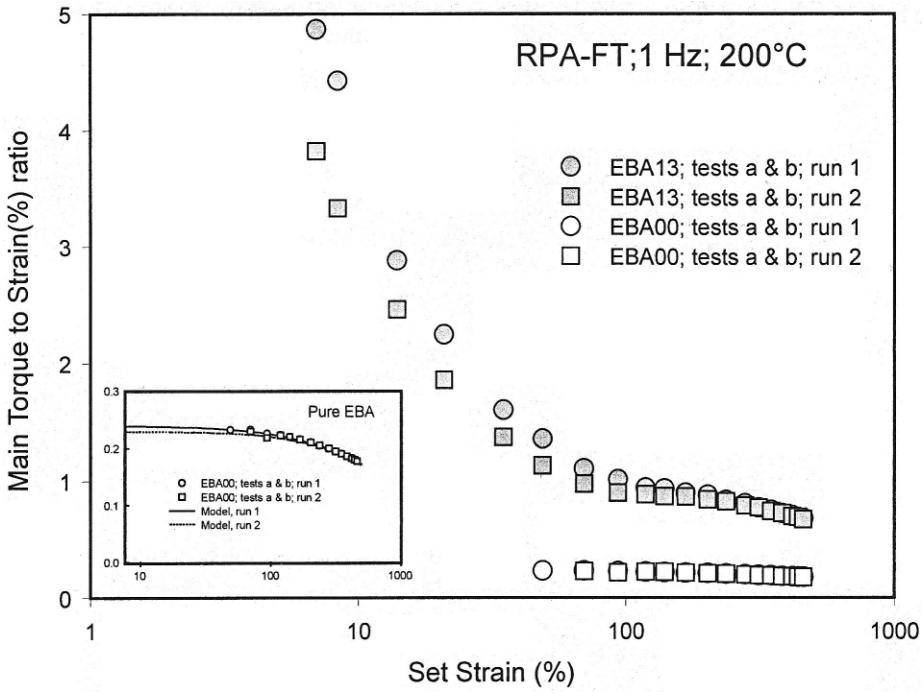

Figure 8 Modulus $\frac{T(\omega_1)}{\gamma}$ versus strain for unfilled and filled EBA.

strain nonlinear effects become dominant. One would interpret such results as the indication that there are interactions between carbon black particles and EBA, strong enough either to resist high strain in the molten state or at least to quickly restore when strain is suppressed. Such interactions would therefore have the capability to notably control the rheological properties of filled EBA materials.

Figure 11 shows the effect of carbon black structure (at constant loading). Again eq. (2) was used to fit data obtained at strain higher than 90%, to yield parameters given in Table V. Only the acetylene black exhibits a clear structure effect, essentially in term of substantially higher modulus. The two furnace blacks show marginal differences in the high strain region but in the low strain region, the unexpected inversion of EBA15 and EBA19, previously seen on RDAII results (see Fig. 3), is also observed here.

Third relative harmonic torque component

FT allows detecting harmonics up to $T(15\omega_1)$ or higher in the torque signal but, above the fifth one, they are becoming too small to be unambiguously distinguished from the noise. The limit of the relative torque harmonic $T(n\omega_1)/T(\omega_1)$ [or $T(n/1)$] is expected to be equal to $1/n$, and $T(3/1)$ is consequently the most intense contribution compared to all other harmonics. The relative third torque harmonic component is therefore the very interesting data for nonlinear viscoelastic characterization.

As previously reported for pure and CB filled elastomers,[6,9] the variation of the relative third torque

TABLE III
Fitting Eq. (2) to Pure EBA Data

Parameters of eq. (1)	Run 1	Run 2
$\left[\frac{T(\omega_1)}{\gamma}\right]_0$	0.24	0.23
$1/A$	1176	1124
B	1.09	1.28
r^2	0.998	0.988

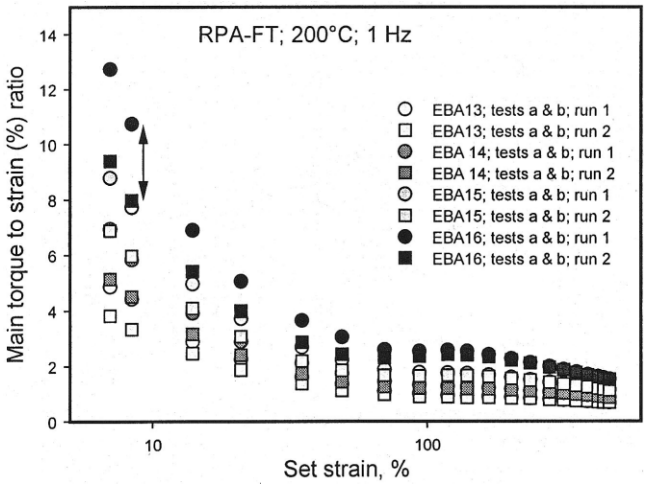

Figure 9 Modulus $\frac{T(\omega_1)}{\gamma}$ versus strain for EBA/CB composites; the double-sided arrow draws the attention on the difference between runs 1 and 2.

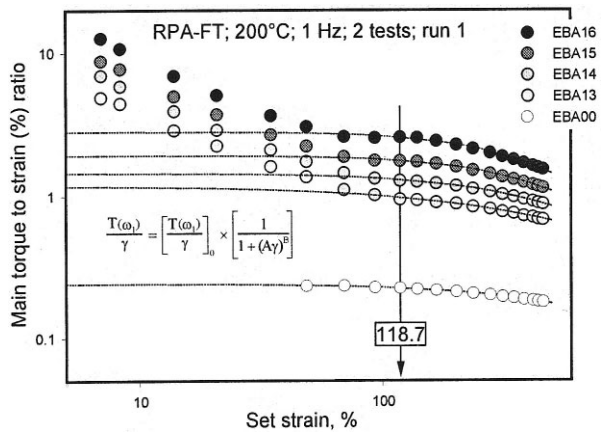

Figure 10 Modulus $\frac{T(\omega_1)}{\gamma}$ versus strain for EBA/CB composites with various filler level, in comparison with pure EBA; only data from run 1 are used for the sake of clarity; the dash lines correspond to curves drawn using eq. (2) and parameters given in Table IV.

harmonic component with the strain amplitude is generally such that an *S*-shape curve is observed, from a (scattered) plateau value at low strain up to a maximum at high strain. Figure 11 shows that such a behavior is indeed observed with the pure EBA sample and results are nicely fitted using the following equation:

$$T(3/1)_\gamma = T(3/1)_{\min} + [T(3/1)_{\max} - T(3/1)_{\min}] \times [1 - \exp(-C\gamma)]^D \quad (3)$$

where γ is the deformation (%), C and D are the fit parameters.† As can be seen, no significant strain history effect is detected pure EBA since data for runs 1 and 2 superimpose well, and the material is well homogeneous (no difference between tests a and b). CB-filled EBA composites exhibit quite an unusual behavior with $T(3/1)$ passing through a maximum before asymptotically reaching a plateau at high strain. In addition, a significant strain history effect is observed at low strain but vanishes as strain increase. Figure 12 shows this behavior in the case of EBA13 sample, which, of course, does not meet the strain dependence modeled by eq. (3).

As shown in Figure 13, CB loading affects the relative third torque harmonic, at least in the low strain region where the maximum is observed, and again significant strain effects are observed. For the sake of clarity, results from runs 1 and 2 are shown separately and the dashed horizontal line underlines the strain history effect in the case of EBA16 (42.5 phr CB). It is fairly obvious that the higher the filler loading, the lower the strain amplitude for the maximum $T(3/1)$ to be observed.

Figure 14 shows the filler structure effect through results obtained with sample EBA 15, EBA19, and EBA28. Whatever be the CB structure, a maximum is observed in the low strain region, with only the acetylene black giving a significant difference. In the high-strain region, the three blacks are distinguished but not in the expected ranking for the two furnace blacks.

TABLE IV
Modeling High Strain Nonlinearity of Filled EBA Composites, using Eq. (2); Effect of CB Loading

Parameters of eq. (2)	EBA00	EBA13	EBA14	EBA15	EBA16
$\left[\frac{T(\omega_1)}{\gamma}\right]_0$	0.24	1.18	1.44	1.91	2.80
$1/A$	1176	662	654	588	510
B	1.09	0.88	1.25	1.50	1.58
r^2	0.998	0.993	0.999	0.996	0.992

DISCUSSION

Our experimental results reveal an unusual complexity of CB effects in EBA-based composites, when compared with more common filled elastomers. Certainly, there is a reinforcing effect at room temperature, with

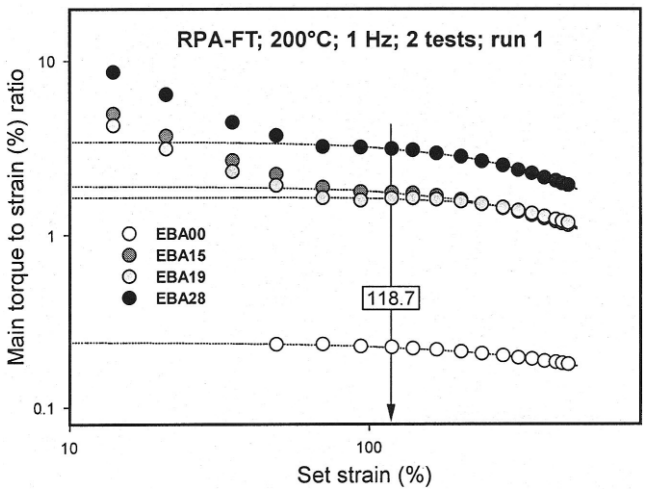

Figure 11 Effect of filler structure on modulus $\frac{T(\omega_1)}{\gamma}$ versus strain for EBA/CB composites (constant filler volume fraction = 0.25), in comparison with pure EBA; only data from run 1 are used for the sake of clarity; the dash lines correspond to curves drawn using eq. (2) and parameters given in Table V.

†In using eq. (3) to model $T(3/1)$ variation with strain, one may express the deformation (or strain) γ either in degree angle or in percentage. Obviously, all parameters remain the same except C, whose value depends on the unit for γ. The following equality applies for the conversion: $C(\gamma, \text{deg}) = C(\gamma,\text{deg}) = 180\alpha/100\pi \times C(\gamma,\%)$, where $\alpha = 0.125$ rad.

loading variation apparently well captured with a model based on mere hydrodynamic consideration and a concern about filler particles anisometry. This is evident from a good fit of the Guth–Gold–Simha equation (eq. (1)) to our experimental data.

Recently, Flandin et al.[11] described solid-state modulus data of CB-filled ethylene–octene elastomer compounds, using the same model, and they argued on the basis of strong particle–polymer interactions. Our results call for similar arguments. Indeed, Figure 2 shows clearly that the reinforcing effect of CB at room temperature is a function of the specific surface area rather than of the aggregate structure. Since the latter is commonly associated with a higher space-filling capability of the CB and thus with an increased contact probability between carbon black particles, one may conclude that particle–particle interactions contribute less to the reinforcing effect than an effect due to restricted mobility of polymer chains in vicinity of the large CB surface area.

At temperatures far above the melting range, however, the reinforcing effect of the different CB types is to some extend reversed (Figs. 3 and 4) showing an increasing impact of the CB aggregate structure. Such a drastic change in the viscoelastic behavior at the melting range has been reported for similar systems, for instance ethylene vinylacetate copolymer filled with acetylene black.[12] The authors concluded that the viscoelastic properties in the solid state are mainly effected by the viscoelasticity of the disperse medium, but in the molten state by the flocculated filler structure. Further, earlier work on EBA–CB compounds[1] has shown that the networking behavior in the melt does not depend on the polymers viscosity or on the test temperature leading to the conclusions that this network is determined by particle–particle links.

In view of the earlier discussion, a consistent picture emerges of reinforcing properties, which are depending on polymer chains with restricted mobility in the solid state, while particle–particle links are dominant in the melt.

Reasons for this change in behavior could be the dramatically enhanced mobility of polymer chains above the melting point that are no longer constrained by their incorporation in crystallite structures. First, a restriction of polymer mobility in vicinity of the CB surface would have less impact; second, more flexible polymer chains are more easily squeezed out from gaps between adjacent CB aggregates under the action of van der Waals forces. Indeed, dielectric experiments on similar systems have shown that capacitive gaps within a filler network are able to close upon thermal annealing above the matrix' melting point, while no such effect has been observed during annealing below the melting range.[13] An implication of the argument above is that the qualitative impact of CB properties on the magnitude of reinforcement is indicative of the reinforcement mechanism in the composite systems studied here. Accordingly, strong impact of CB surface area and activity as measured in the solid state is indicative of restrictions in polymer mobility in vicinity of the CB surface, and a strong impact of the CB structure as measured in the molten state is indicative of predominant filler–filler interactions. From this not only changes in the reinforcing mechanism upon a polymer phase transition can be concluded, but also it further points at an effect of the flow conditions. For instance, the higher structured furnace black 1 reinforces less than the lower structured furnace black 2, in dynamic mechanical testing of the melt, but reinforces stronger in capillary rheometry. Interestingly, RPA-FT data seem to indicate this kind of transition from one mechanism to the other upon increasing strain levels. At small strains composites with the lower structured furnace black 1 have a larger modulus than the higher structured furnace black 2. At large strain the order is reversed.

Solid-state data suggest that there are still important crystalline regions in EBA at room temperature, even

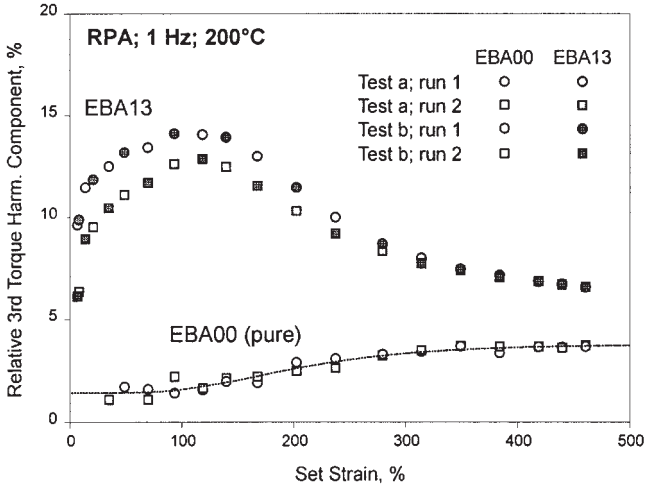

Figure 12 Relative third torque harmonic versus strain for unfilled EBA (EBA00) and 33.2 furnace CB-filled EBA (EBA13); two samples tested; the dashed curve correspond to EBA00 data fit with eq. (3).

TABLE V
Modeling High Strain Nonlinearity of Filled EBA Composites, using Eq. (2); Effect of CB Structure (at Constant Loading)

Parameters of eq. (2)	EBA00	EBA15	EBA19	EBA28
$\left[\frac{T(\omega_1)}{\gamma}\right]_0$	0.24	1.91	1.65	3.45
$1/A$	1176	588	681	534
B	1.09	1.50	2.20	1.52
r^2	0.998	0.996	0.986	0.998

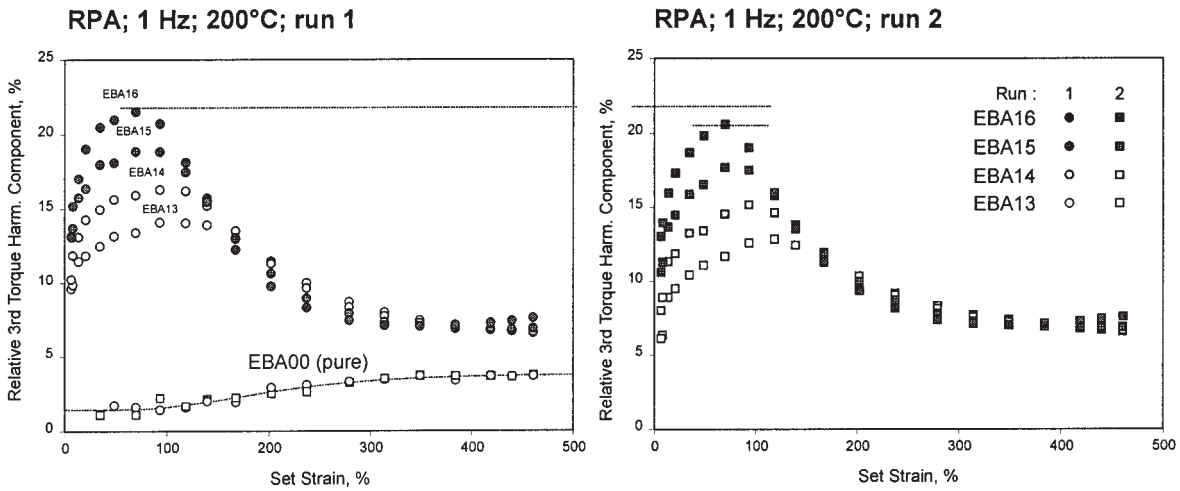

Figure 13 Effect of CB loading on the relative third torque harmonic component of filled EBA composites; two samples were tested; results from run 1 are given in the left part of the figure; results from run 2 in the right part.

if as shown in a paper by Feller et al.,[14] increasing the acrylate content in EPA tends to decrease all crystalline characteristics. These authors explain CB activity during the crystallization process through the assumed existence of molecular interactions between CB particles and acrylate groups rather than by a pure nucleating effect. However, 3% butyl acrylate is not much, and surely our EBA is crystalline at room temperature. Therefore, one would expect CB particles to be concentrated in amorphous regions, thus leading to a highly complex morphology with at least three phases: PE-rich crystallites (no black in it), BA-rich amorphous, and carbon black. In terms of modulus, the ranking is obviously CB > crystallites > amorphous).

As semicrystalline character is kept in EBA–CB composites, it is fairly obvious that filler particles concentrate in amorphous regions of the material, which are also BA-rich regions. At room temperature, such composites can therefore be viewed as basically a dual-phase system consisting of ethylene segments (PE)-rich crystallites and CB-rich amorphous BA regions. Solid-state mechanical properties are therefore reflecting the reinforcement by CB of the amorphous regions of the semicrystalline copolymer. As temperature increases, crystallites progressively melt allowing a pseudofluid state to be achieved, but the dual-phase morphology is essentially kept, since all the properties of the solid state are recovered by simply cooling down the melt. Owing to their heterogeneous nature, molten EBA–CB composites exhibit intrinsically nonlinear viscoelastic properties, whose roots are in the morphology of the material. Under increasing (dynamic) strain, such a complex dual-phase molten system is consequently exhibiting a response that is initially characterized by a contribution from PE-rich

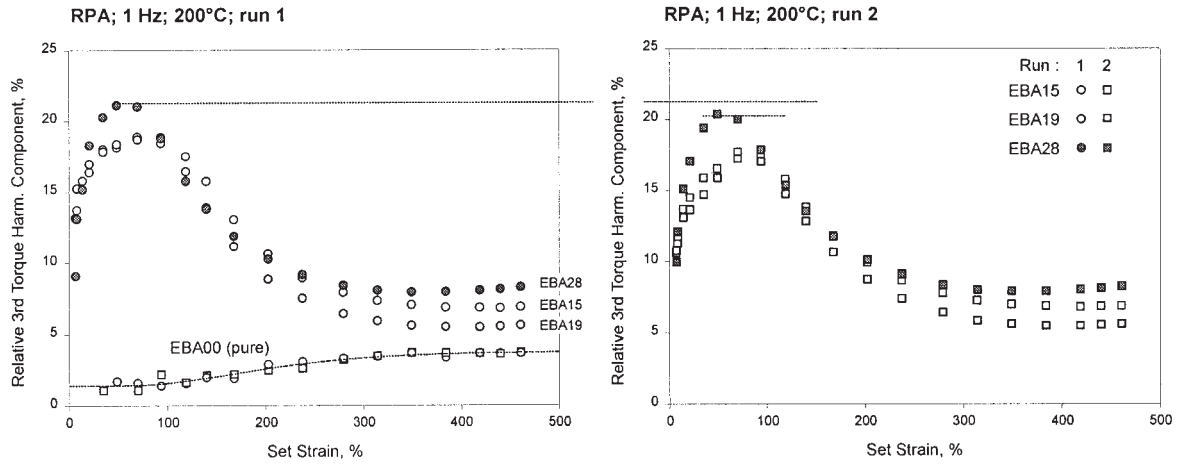

Figure 14 Effect of CB structure on the relative third torque harmonic component of filled EBA composites.; two samples were tested; results from run 1 are given in the left part of the figure; results from run 2 in the right part.

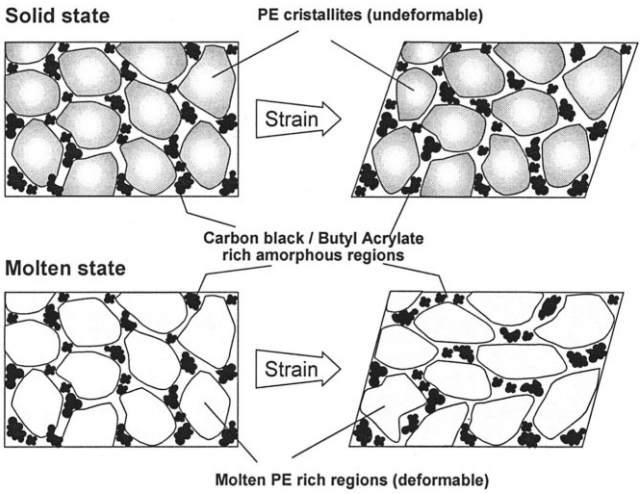

Figure 15 Pictorial representation of the likely morphology of CB-filled EBA composites in both the solid and molten states.

regions, easier to deform than CB-rich amorphous BA regions, before the expected response of the filled BA phase is observed. Figure 15 offers a pictorial representation of CB-filled EBA in both the solid and molten state.

CONCLUSIONS

FT rheometry, combined with other techniques, allows a very fine investigation of complex polymer systems such as molten CB/EBA composites. A number of accurate and reproducible results are obtained despite the complexity of the tested materials. FT rheometry appears particularly sensitive to such a complexity with namely typical variations of torque harmonics as dynamic torsional strain is increased at constant frequency and temperature. How CB particles are distributed in the material is the key to understand experimental results, both in solid and in molten state.

In the solid state, EBA–CB composites exhibit viscoelastic properties that are essentially dominated by the CB-rich BA phase, while in the molten state, the PE-rich phase contributes significantly to the initial response in such a manner that a certain strain limit has to be reached before the filler reinforcing effect in the BA phase is observed. Such an interpretation of our results is consistent with the modification in electrical properties through melting and cooling, as previously reported.

This paper finds its roots in a spontaneous collaboration between the authors which thank Borealis AB, Sweden, for the permission to publish it.

References

1. Jäger, K.-M.; McQueen, D. H. Kautsch Gummi Kunstst 1999, 52, 734.
2. Jäger, K.-M.; Eggen, S. S. Polymer 2004, 45, 7681.
3. Leblanc, J. L. Prog Polym Sci 2002, 27, 627.
4. Sternstein, S. S.; Zhu, A. Macromolecules 2002, 35, 7262.
5. Leblanc, J. L.; de la Chapelle, C. Rubber Chem Technol 2003, 76, 287.
6. Leblanc, J. L. J Appl Polym Sci 2003, 89, 1101.
7. Guth, E.; Simha, R. Kolloid-Zeitschrift 1936, 74, 266.
8. Guth, E.; Gold, O. Phys Rev 1938, 53, 322.
9. Wolff, S.; Wang, M.-J. In Carbon Black Science and Technology, 2nd ed.; Donnet, J.-B., Bansal, R. C., Wang, M.-J., Eds.; Marcel Dekker: New York, 1993.
10. Leblanc, J. L. J Appl Polym Sci, to appear.
11. Flandin, L.; Hiltner, A.; Baer, E. Polymer 2001, 42, 827.
12. Amari, T.; Uesugi, K.; Suzuki, H. Prog Org Coating 1997, 31, 171.
13. Jäger, K.-M.; McQueen, D. H.; Vilcakova, J. J Phys D: Appl Phys 2002, 35, 1068.
14. Feller, J. F.; Linossier, I.; Pimbert, S.; Levesque, G. J Appl Polym Sci 2001, 79, 779.